# Temperature Effects on Electrophoresis

Anita Rogacs and Juan G. Santiago*

Department of Mechanical Engineering, Stanford University, Stanford, California 94305, United States

S *Supporting Information*

ABSTRACT: We present a model capturing the important contributors to the effects of temperature on the observable electrophoretic mobilities of small ions, and on solution conductivity and pH. Our temperature model includes relations for temperature-dependent viscosity, ionic strength corrections, degree of ionization (pK), and ion solvation effects on mobility. We incorporate thermophysical data for water viscosity, temperature-dependence of the Onsager—Fuoss model for finite ionic strength effects on mobility, temperature-dependence of the extended Debye—Huckel theory for correction of ionic activity, the Clarke—Glew approach and tabulated thermodynamic quantities of ionization reaction for acid dissociation constants as a function of temperature, and species-specific, empirically evaluated correction terms for temperature-dependence of Stokes' radii. We incorporated our model into a MATLAB-based simulation tool we named Simulation of Temperature Effects on ElectroPhoresis (STEEP). We validated our model using conductivity and pH measurements across a temperature variation of 25−70 °C for a set of electrolytes routinely used in electrophoresis. The model accurately captures electrolyte solution pH and conductivity, including important effects not captured by simple Walden-type relations.
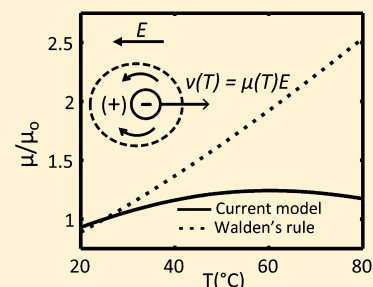
The fields of drug discovery, genetics, proteomics, toxin detection, and food analysis, among others, employ electrophoretic separation as a workhorse analysis technique. Electrophoresis methods include capillary electrophoresis (CE), isotachophoresis (ITP), isoelectric focusing (IEF), and temperature gradient focusing (TGF); all of which rely on differences between analyte electrophoretic mobilities for separation.[1] A wide range of these methods use temperature variation to improve performance and enable new functionalities. Likely the most common utility of elevated temperature is speeding up electrophoretic separations.[2−4] For example, compared to room temperature, CE separation times can be reduced by 2.5-fold at 70 °C.[1,4] Other uses include improvement of resolution by changing the degree of ionization of analytes,[5−11] and manipulation of nucleic acid secondary structure[4,12] or protein conformation.[13,14] TGF specifically relies on temperature gradients to focus and separate analytes.[15,16] Temperature effects on electrophoresis can also cause nonideal behavior, including experimental variability, Joule-heating-induced zone dispersion,[17−19] and increased electromigration dispersion.[20,21] As we will discuss, a 5 °C temperature change can produce as much as 0.1 units change in the pH, and over 25% change in observable mobility of analytes at specific conditions.

The observable mobility of an ion depends on the solvent viscosity, ionic strength of the electrolyte solution, the degree of ionization of the ion, and solvation of the ion. The temperature sensitivity of viscosity, varying 2% per °C near room temperature,[22] has a marked influence on electrophoretic mobility, and is typically modeled using the so-called Walden's rule. Similarly, the strong temperature dependence of ion dissociation constant (K) can have pronounced influence on the degree of ionization and so the observable mobility of an

ion. We here refer to only acid dissociation constants, K_a, and never the related base equilibrium constants, $K_b = K_W/K_a$, so we drop the "a" with no ambiguity.) As we shall discuss, neglecting this effect can result in gross errors in prediction for buffer pH (e.g., greater than 0.5 pH unit), buffer conductivity (>100%) and effective mobility of analytes (>400%) at 80 °C (all relative to room temperature, see Supporting Information for details). Although commonly used, Walden's rule does not hold for some small ions like potassium or chloride, which are poorly hydrated at low temperatures. Neglecting temperature dependence of hydration shell for small ions (e.g., K^+ or Cl^-) can result inasmuch as ~20% error in the predicted absolute mobilities over a 70 °C change.[23]

In general, the contributions to electrophoretic mobility from temperature dependence of electrolyte ionization, ionic strength corrections, and ion solvation, have been largely overlooked.[24] In Table 1, we show the results of a brief survey of temperature effects addressed by published models, and compare these to the current work. Most of these studies explored temperature effects on one of two types of electrolyte properties, but not on both. These two types are (1) weak electrolyte pK (e.g., Okamoto et al.[25]) and (2) the "actual" mobility of fully ionized electrolytes. (e.g., Anderko and Lencka[26]) In Table 1, we indicate with a dash if temperature effects on an electrolyte property were not considered in (or if property was not relevant to) the study. Despite the importance and prevalence of the various effects, we found no comprehensive models which capture all important contributors of temperature to ion (weak and strong electrolyte)

Table 1. Examples of Temperature Models of Aqueous Electrolyte Solutions from the Last 25 Years[a]

references	acid dissociation constant, $pK(T)$	actual mobility, $\mu°(T)$
Clancy (1987)[27]	dpK/dT, ISC-pK	–
Rush et al. (1991)[13]	–	W
Whang and Yeung (1992)[10]	dpK/dT	W
Chang and Yeung (1993)[11]	dpK/dT	W
Beynon and Easterby (1996)[28]	dpK/dT	–
Okamoto et al. (1997)[25]	pKC-VH, ISC-pK	–
Anderko and Lencka (1997)[26]	–	W, ISC-μ, SSC
Fukada and Takahashi (1998)[29]	pKC-VH, pKC-CG	–
Rochu et al. (1999)[14]	–	W
Wang and Tsao (2004)[30]	–	W
Reijenga et al. (2007)[31]	dpK/dT	W
Evenhuis et al. (2007)[24]	–	W, ISC-μ
Mandaji et al. (2009)[32]	dpK/dT	W
Milanova et al. (2011)[33]	–	W
current work	pKC-VH, pKC-CG, ISC-pK	W, ISC-μ, SSC

[a]Effects captured by each model are categorized into two types: pK or actual mobility, $\mu°$ corrections. Abbreviation "dpK/dT" indicates that only tabulated values of this slope were presented. "pKC-VC" and "pKC-CG" represent models which account for temperature dependence of pK using van't Hoff or the higher accuracy Clark–Glew model, respectively. Viscosity corrections using of the Walden rule type are indicated with "W". We also list models which account for the temperature dependence of ionic strength corrections of activity coefficient (ISC-pK) and actual mobility (ISC-μ).

mobilities and electrolyte solution conductivity and pH. For example, we know of no studies of temperature effects on electrolyte properties which capture both solvation effects and dissociation effects, nor temperature models including ionic strength corrections to both pK and absolute mobility.

A fully comprehensive model for temperature effects on electrophoretic mobility is challenging as temperature change may lead to ad hoc and difficult-to-predict effects including variations in DNA gel migration dynamics,[34] sieving matrix properties,[35] and electroosmotic flow (EOF).[36] However, the basic phenomena associated with the mobility of weak electrolyte ions in water and the electrolyte solution pH are addressable using a fairly general model. These basic phenomena can be used to directly predict temperature-dependence of electrolyte solution pH and conductivity, and analyte mobility; likely the most relevant parameters in any separation assay.

We here present a fairly comprehensive model to quantify the effects of temperature on analyte mobility and solution conductivity. Our model includes temperature dependence of (1) viscosity, (2) ionic strength corrections on both mobility and pK, (3) degree of ionization (pK), and (4) ion solvation effects on mobility. Our model leverages thermophysical data for water viscosity;[22] temperature dependence of the Onsager–Fuoss model for finite ionic strength effects on mobility;[37,38] temperature dependence of the extended Debye–Huckel theory for correction of ionic activity;[38,39] the Clarke–Glew generalized approach[40] to predict $K(T)$ from tabulated thermodynamic properties;[41] and species-specific, empirically evaluated correction terms for temperature-dependence of Stokes' radii of 11 common small ions.[23] We validated our model using a series of conductivity and pH measurements

across a temperature variation of 25–70 °C for a set of electrolyte solutions routinely used in electrophoresis.

■ THEORY

We define the mobility of species i, μ_i, as the drift velocity of the ion through the solvent divided by the applied electric field magnitude, E. As usual, we define the "limiting" (or absolute) mobility of an ion in solution as the mobility that a fully ionized ion would take on in the limit of infinite dilution and with known integer values of its valence. At finite ionic strength, the 'actual' mobility of an ion is obtained by considering the effect of the ionic atmosphere on the movement of the fully ionized ion.[42] For weak electrolytes, the observed or 'effective' electrophoretic mobilities are dependent on the degree of dissociation of the analyte. We here summarize the models describing the temperature effect on limiting, actual, and effective ionic mobilites. These include temperate dependent variations of viscosity, dielectric constant, ion solvation, ionic strength effects, and dissociation constants.

WALDEN'S RULE. The limiting mobility, μ_i^o, of ionic species i, can be formulated as a balance between the applied electric force and retarding frictional forces acting on the ion. For infinite dilution, this balance can be approximately modeled by a form of Stokes' drag law as follows:

$$\mu_{i,z}^0 = \frac{z_i e}{6\pi\eta r_{z,i}} \tag{1}$$

Here, z_i is the valence of the ion, e is the elementary charge (electron charge), η is the dynamic viscosity of the solvent, and $r_{z,i}$ is the Stokes' (or hydrodynamic) radius of the solvated ion. Stokes' law describes the drag on a sphere in a simple, continuum fluid flow in the limit of negligible inertial effects. The Stokes's radius of an ion can be interpreted as the radius of a sphere with the same viscous drag as the ion. Because of noncontinuum effects and the complex interactions between the ion, nearby counterions, and the solvent molecules, the Stokes' radius is only roughly related to other measures of ion dimensions, such as the crystallographic radius. Even in the limit of infinite dilution, the Stokes' radius of an ion is therefore an empirically determined quantity which accounts for the nonspherical nature of the ion and the effect of its hydration shell. This quantity is often measured at some reference temperature, θ.

Treatment of limiting ion mobility as a balance between electric force and a drag law from continuum flow theory leads to an approximate relation between mobility and solvent viscosity. For aqueous solutions, we can leverage empirical correlations for water viscosity, η, as a function of temperature, T, as follows:[22]

$$\log_{10}\left\{\frac{\mu(T)}{\mu(20\,°C)}\right\} = \frac{20-T}{T+96}\{1.2378$$
$$- 1.303 \times 10^{-3}(20-T) + 3.06$$
$$\times 10^{-6}(20-T)^2 + 2.55 \times 10^{-8}(20-T)^3\} \tag{2}$$

This useful correlation covers the temperature range of −8 °C $\leq T \leq$ 150 °C with an uncertainty of ± 0.26%. Equation 1 suggests that a change in the viscosity of the medium will lead to an approximately inversely proportionate change in the limiting mobility of the ion. This leads to the definition of the Walden's rule or Walden's product, $WP_{i,z} = \eta\mu_{i,z}^o$.[43] Walden's rule assumes $WP_{i,z}$ is independent of temperature for each ion

and can be used to correct the limiting mobility of ions, $\mu_{i,z}^o$, evaluated at the reference temperature, θ, as follows:

$$\mu_{i,z}^0(T) = \alpha \mu_{i,z}^0(\theta) \quad (3)$$

where $\alpha = \eta(\theta)/\eta(T)$. (We will use T in parentheses periodically to emphasize the temperature dependence of a variable.) Walden's rule is useful in gaining physical intuition into solvent viscosity effects on limiting ion mobility. However, as we discuss below, application of Walden's rule alone to predict ion mobility can result in severely erroneous mobility predictions at a given operating temperature, T.

Ion Solvation Effect on Limiting Ion Mobility. As we have mentioned, the idea of a Stokes' radius and Walden's rule in determining limiting ion mobility has only limited use. Quantitatively, the Walden product in eq (3) is known to vary with temperature, particularly for small ions. This inaccuracy is due to the complexity of ion−solvent interactions, which is only approximately captured by a continuum drag law in terms of solvent viscosity. We here present a summary discussion of the physicochemical nature of these interactions and then propose a set of empirical corrections for prediction of limiting ion mobilities for common small ions. We incorporate these empirical corrections in our model. E.R. Nightingale (1959) studied and showed the importance of ion−solvent interactions in the prediction of limiting ion mobility. Nightingale[23] provided empirical data for the Walden product (in water) of varying Stokes radii as a function of temperature. The data show that this temperature dependence is highly specific to ions. The typical trend is for Walden product, WP, to decrease with increasing temperature, and the effect is most pronounced for smaller ions, such as chloride, potassium, and nitrate. Nightingale qualitatively attributed this effect to the ion-dependent disruption of water structure for ions of varying size and shape. A review of such empirical data for limiting ion mobility and the theory behind solvent−ion interactions was presented by Sadek.[44] Sadek similarly described these phenomena in the context of "structure making" or "structure breaking" properties of ions and the solvent. Water possesses quartz-like molecular structure, a tethrahedral coordination, in which each water molecule can participate in two collective hydrogen bonds. This permits the existence of cavities of various sizes. Sadek classified ions into three categories associated with the relative size of the ions versus the size of these cavities in the water structure. These hypotheses propose that the small ions occupy these cavities in the water, and the relative size of the ion and the cavity helps determine the degree of order in the hydration shell around the ion. Stokes' type law is most useful and accurate for ions whose size is relatively large compared to the dimensions of these cavities.

The current theories of ion solvation are useful in providing intuition as to the ion-specific nature of temperature dependence of limiting mobility. However, despite significant work in the field,[44] a theory for quantitative prediction of these effects is not available. Indeed, the physicochemical nature of ion−solvent interactions is not well understood, and considered one of the most difficult problems associated with the study of electrolyte solutions.[44−46] We here therefore take the approach of providing ion-specific empirical corrections for the effect of solvation on limiting ion mobility. To this end, we exploit the clear trend in the data that the smallest ions are subject to the strongest temperature dependence of limiting ion mobility (and WP). We formulate this correction in terms of empirical data

for temperature dependence of the ion-specific, valence-normalized Walden's product, $WP_{i,z} = \lambda_{i,z}^\circ \eta^\circ / z_i$, expressed in terms of the limiting conductivity, $\lambda_{i,z}^\circ$, for 11 species,[23] where limiting ionic equivalent conductivity is defined as $\lambda_{i,z}^\circ = 0.820 z_i/(r_{i,z}\eta^\circ)$. Here, we define the solvation correction term for ion i as $\beta_{i,z} \equiv (\lambda_{i,z}^\circ(T)\eta^\circ(T))/(\lambda_{i,z}^\circ(\theta)\eta^\circ(\theta))$, which we use to correct for ion-solvation associated temperature effects on limiting mobility. At the operating temperature, T, we therefore evaluate the limiting mobility as

$$\mu_{i,z}^\circ(T) = \alpha\beta_{i,z}\mu_{i,z}^\circ(\theta) \quad (4)$$

where $\mu_{i,z}^\circ(\theta)$ is the limiting mobility of an ion measured at the reference temperature, θ, and α accounts for the inversely proportionate change in the limiting mobility of the ion with viscosity. The 11 cases for which we provide the temperature-dependent correction term, $\beta_{i,z}$ include chloride, sodium, potassium, nitrate, lithium, magnesium, perchlorate, rubidium, cesium, calcium, silver, and sulfate. Chloride, potassium, perchlorate, and nitrate particularly exhibit strong temperature dependence and are also common electrolyte ions. Our experimental validation of our model shows that neglecting these ion solvation corrections can result inasmuch as 20% error in prediction of ion mobilities (e.g., for the case of K$^+$ over a 70 °C change).

Ionic Strength Correction of Limiting Mobility: Actual Ion Mobility. So far, we have discussed ion mobilities for the case of fully ionized ions at infinitesimal ionic strength. At finite ionic strength, the presence of an ionic atmosphere around the ion reduces (in all cases) the limiting ion mobility to the so-called actual mobility. There is a wide body of accepted quantitative theory describing these phenomena.[42] Here, we adopt the extended Onsager−Fuoss model, which is applicable to an arbitrary mixture of species at ionic strengths up to 100 mM[47] and can be formulated as follows:

$$\mu_{i,z}(T) = \alpha\beta_{i,z}\mu_{i,z}^\circ(\theta) - (A\alpha\beta_{i,z}\mu_{i,z}^\circ(\theta) + B)$$
$$\frac{\sqrt{\Gamma}}{1 + \frac{aD}{\sqrt{2}}\sqrt{\Gamma}} \quad (5)$$

where

$$\Gamma = \sum_{i=1}^{s}\sum_{z=n_i}^{p_i} z^2 c_{i,z}$$

Here, s is the number of species, z_i is the charge number of the i-th ionic species, ε the permittivity of solution, k is the Boltzmann constant, e is the elementary charge, N_{AV} is the Avogadro constant, T is the temperature of the solution, and Γ is twice ionic strength, I. The coefficients C_n and the vectors R^n are given by Onsager and Fuoss.[37]

We note our formulation of the extended Onsager−Fuoss differs from previous versions (e.g., as used by Bahga and Santiago[42]) in employing the prefactors α and $\beta_{i,z}$ to account for temperature effects. Recall, the temperature-dependent term, α, accounts for the inversely proportionate change in the limiting mobility of the ion with viscosity; and $\beta_{i,z}$, is a modification of Onsager-Fuoss model, which we propose here to correct for ion solvation effects.

We use a standard approach to account for the ionic-strength-related reduction in mobility. This reduction can be attributed primarily to two factors. The first is represented by the temperature dependent term, A. This is the so-called

relaxation effect which captures the polarization of the ionic atmosphere surrounding the ion, which acts to lower the effective, local electric field experienced by the ion. By definition, the absolute temperature appears in parameter A, which is defined as

$$A = z_i \frac{e^3}{12\pi} \sqrt{\frac{N_{AV}}{(\epsilon k T)^3}} \sum_{n=0}^{\infty} C_n R_i^n \tag{6}$$

where ϵ is the water dielectric constant, whose temperature dependence can be approximated by the following correlation[48]

$$\epsilon = 249.21 - 0.79069T + (0.72997 \times 10^{-3})T^2 \tag{7}$$

where A depends on temperature as, $1/(\epsilon T)^{3/2}$, a fairly weak temperature dependence.

The second effect associated with ionic strength reduction of mobility is captured by the parameter B. This is the so-called electrophoretic effect which is associated with the drag force exerted by the moving counterion cloud on the central ion. Water viscosity and dielectric constant each impact the magnitude of this drag force, formulated as

$$B = |z_i| \frac{e^2}{6\pi\eta} \sqrt{\frac{N_{AV}}{\epsilon k T}} \tag{8}$$

which makes B a strong function of temperature.

The aD term in the extended Onsager−Fuoss model takes into account the finite size of ions, where a represents the mean distance of the closest approach for the ions (distance from center of the central ion to the start of the ionic atmosphere).[37,49] The value assigned to aD is empirically determined, and estimated to lie between 1 and 2 dm$^{3/2}$ mol$^{-1/2}$. For most electrolytes, the recommended approximation for aD is 1.5 dm$^{3/2}$ mol$^{-1/2}$, which we adopt here. D is defined as

$$D = \sqrt{\frac{2e^2 N_{AV}}{\epsilon k T}} \tag{9}$$

and so has a weak temperature dependence, varying only 2.7% over 60 °C change.[38] This change is smaller than the variation among reported values of aD. Therefore, in our model we assume a constant value of 1.5 dm$^{3/2}$ mol$^{-1/2}$ for aD for all temperatures, as recommended by Grenthe and Plyasunov.[38]

Degree of Ionization: Effective Mobility. *van't Hoff (ΔT < 20 °C).* The effective (observable) mobility of a weak electrolyte is determined by its degree of ionization. Prediction of effective mobility for weak electrolytes is therefore a function of the acid−base equilibrium of the entire ion mixture. See Persat et al.[50] for a detailed discussion of the effect of ionization on observable mobility. Using the notation of Stěrdý et al.[51,52] and Bercovici et al.,[52] we can express the total concentration of ionic species i, c_i, as the sum of its constituent ionization states as follows:

$$c_i = \sum_{z=n_i}^{p_i} c_{i,z} \tag{10}$$

Here $c_{i,z}$ is the concentration of species i of an ionic state with valence z. The limits specify the maximum, p_i, and minimum, n_i, valance values of species i. The activities of two consecutive ionic states of species i are related by the thermodynamic equilibrium constant $K_{i,z}$ as follows:[42,53]

$$K_{i,z}(T) = \frac{a_{i,z} a_H}{a_{i,z+1}} = \frac{\gamma_{i,z} \gamma_H}{\gamma_{i,z+1}} \frac{c_{i,z} c_H}{c_{i,z+1}} \tag{11}$$

where c_H is the concentration of H$^+$ and $\gamma_{i,z}$ is the activity coefficient of the z-th ionic state of species i. Extensive tabulations of thermodynamic data on ionization reactions are available for a large number of acids and bases.[41,54] A particularly important subset of data belongs to species used as buffers in aqueous solutions. Accurate prediction of their pK, p$K_{i,z}(T) = -\log_{10} K_{i,z}(T)$, at a given operating temperature is critical in applications requiring knowledge and precise control of pH and ionic strength. The thermodynamic equilibrium constant, $K_{i,z}(T)$ is a thermodynamic quantity which depends on the standard free enthalpy, $\Delta H_{i,z}^\circ$, and entropy, $\Delta S_{i,z}^\circ$, of ionization of the electrolyte species. This relation can be expressed as follows:

$$pK_{i,z}(T) = \frac{\Delta G_{i,z}^\circ}{2.303 RT} = -\frac{\Delta H_{i,z}^\circ - T\Delta S_{i,z}^\circ}{2.303 RT} \tag{12}$$

where the coefficient 2.303 arises from the conversion of natural to 10-base logarithm. Over very small temperature differences (ΔT < 5 °C), pK dependence on temperature is approximately linear, therefore the empirically determined temperature derivative, dp$K$/dT (e.g., see Persat et al.,[53] who reported dp$K$/dT for many common electrolyte species) can be used to predict variations in pK at the operating temperature.

In the case of moderate temperature variations (5 °C < ΔT < 20 °C), we recommend the use of the simple integrated van't Hoff equation, which assumes that the standard enthalpy change, $\Delta H_{i,z}^\circ$, and the standard entropy change, $\Delta S_{i,z}^\circ$, are constant with temperature. Differentiating eq 12 with respect to temperature, and then integrating from θ to T gives

$$pK_{i,z}(T) = pK_{i,z}(\theta) - \frac{\Delta H_{i,z}^\circ(\theta)}{2.303 R} \left(\frac{1}{\theta} - \frac{1}{T} \right) \tag{13}$$

Equation 13 can be used to evaluate $pK_{i,z}$ at the operating temperature, T, provided that we know the $pK_{i,z}(\theta)$ and $\Delta H_{i,z}^\circ(\theta)$. Goldberg et al.[41] and Christensen et al.[54] have an extensive list for empirically determined thermodynamic properties (including $pK_{i,z}$ and $\Delta H_{i,z}^\circ$) of ions in aqueous solution (at $\theta = 298.15K$). Our buffer simulation tool (see end of Theory Section) includes a database of $pK_{i,z}(\theta)$ and $\Delta H_{i,z}^\circ(\theta)$ for over 100 species.

Clarke and Glew Relation (T < 100 °C). Over wider temperature ranges, we recommend the Clarke and Glew approach,[40] which accounts for the temperature dependence of the standard enthalpy, $\Delta H_{i,z}^\circ$, and the standard entropy change, $\Delta S_{i,z}^\circ$, when deriving the representative function for $pK_{i,z}(T)$, from eq 12. The temperature gradient of $\Delta H_{i,z}^\circ$ of species i, with valence z,

$$\left(\frac{\partial \Delta H_{i,z}^\circ}{\partial T} \right)_p = (\Delta C_p^o)_{i,z} \tag{14}$$

defines another thermodynamic quantity, the change in heat capacity at constant pressure, $\Delta C_{p,i,z}^o$.[55] For many ionization reactions, the temperature dependence of $\Delta S_{i,z}^o$ also reflects a nonzero $\Delta C_{p,i,z}^o$ associated with such reactions.[55] For a reversible process at constant pressure

$$\left(\frac{\partial \Delta S^{\circ}_{i,z}}{\partial T}\right)_p = \frac{(\Delta C^{\circ}_p)_{i,z}}{T} \tag{15}$$

Assuming that $\Delta H^{\circ}_{i,z}(T)$ and $\Delta C^{o}_{p,i,z}(T)$ are well-behaved functions of T, their value can be properly expressed as perturbations on the tabulated values of $\Delta H^{\circ}_{i,z}(\theta)$ and $\Delta C^{o}_{p,i,z}(\theta)$, respectively, by Taylor's series expansion (see Clarke and Glew[40] for derivation). The dissociation constant, $pK_{i,z}(T)$, can then be expressed at the operating temperature, T, as follows:

$$
\begin{aligned}
pK_{i,z}(T) = {} & pK_{i,z}(\theta) - \frac{\Delta H^{\circ}_{i,z}(\theta)}{2.303R}\left(\frac{1}{\theta} - \frac{1}{T}\right) \\
& - \frac{\Delta C^{\circ}_{p,i,z}(\theta)}{2.303R}\left\{\left(\frac{\theta}{T}\right) - 1 + \ln\left(\frac{T}{\theta}\right)\right\} \\
& - \frac{\theta}{4.606R}\frac{\partial \Delta C^{\circ}_{p,i,z}(\theta)}{\partial T}\left\{\left(\frac{T}{\theta}\right) - \left(\frac{\theta}{T}\right)\right. \\
& \left. - 2\ln\left(\frac{T}{\theta}\right)\right\}
\end{aligned}
\tag{16}
$$

Additional terms involving higher order derivatives of $\partial \Delta C^{o}_{p,i,z}(\theta)/\partial T$ can be added to the right-hand side of eq 16.[40] Since the quantity $\partial \Delta C^{o}_{p,i,z}(\theta)/\partial T$ and its higher derivatives require difficult measurements of the third and higher derivative of $pK_{i,z}(T)$ versus temperature, they are not known for most ionization reactions.[41] However, in our own review of these issues, we found that for operating temperatures typically encountered in electrophoresis and focusing assays ($T < 100$ °C), the terms including temperature derivatives of $\Delta C^{\circ}_{p,i,z}$ have negligible contributions to $pK_{i,z}(T)$. Our buffer simulation tool (see end of Theory Section) includes a database of $pK_{i,z}(\theta)$, $\Delta H^{\circ}_{i,z}(\theta)$, and $\Delta C^{\circ}_{p,i,z}(\theta)$ for 36 common species.

Temperature Effects on Ionic Strength Correction of Activity Coefficients. For dilute solutions, concentrations can be used in place of chemical activities, a, in eq 11. However, at significant ionic strengths, the activity coefficients, γ, are smaller than unity, and their ionic strength and temperature dependence must be taken into account. Here we express the apparent thermodynamic equilibrium constant, $\tilde{K}_{i,z}(T)$, which is evaluated from the measured concentrations, eq 17, as a function of the temperature dependent equilibrium constant, $K_{i,z}(T)$, (eqs 12 or 16) and the ionic strength and temperature-dependent activity coefficients

$$\tilde{K}_{i,z}(T) = \frac{\gamma_{i,z+1}}{\gamma_{i,z}\gamma_H}K_{i,z}(T) = \frac{c_{i,z}c_H}{c_{i,z+1}} \tag{17}$$

Our model uses extended Debye–Huckel theory to capture the ionic strength and temperature effects on activity coefficients[39] as follows:

$$
\log \gamma_{i,z}(T) = -z^2\frac{A_{DH}\sqrt{I}}{1 + aD\sqrt{I}} + bz^2 I,
$$
$$
I = \frac{1}{2}\sum_{i=1}^{s}\sum_{z=n_i}^{p_i}z^2 c_{i,z} \tag{18}
$$

The first term on the right-hand side is the Debye–Huckel term, which accounts for long-range, nonspecific, electrostatic interactions. The value of A_{DH} at the reference temperature of

25 °C, is 0.5012 dm$^{1/2}$ mol$^{-1/2}$ and its temperature dependence is given by

$$A_{DH} = \frac{e^3 N_{Av}^{1/2}}{4\pi\sqrt{2}(\epsilon k T)^{3/2}\ln 10} \tag{19}$$

As expected from the $1/(\epsilon T)^{3/2}$ dependence, the variation of this parameter with temperature is relatively small.[39] Extended Debye–Huckel theory also takes into account contributions from the finite nature of ions in the denominator (see discussion on term aD in section 2.3). The second term on the right-hand side of eq 18 accounts for specific, short-range, nonelectrostatic interactions occurring at high ionic strengths, as approximated by a linear, empirical correction term, b. The value of b at 25 °C is 0.1 dm^3 mol^{-1}. b values at temperatures other than 25 °C depend on the value adopted for aD.[38] However, the variation of b with temperature, $(db/dT)_p$, is less than 0.005 dm^3 mol^{-1} K^{-1}.[56,57] The temperature effect of b is therefore very often negligible. For example, in the range 0 to 50 °C, assuming a constant value of b, the error in $\log \gamma_{i,z}/I$ will be less than 0.13 dm^3 mol^{-1}. This corresponds to a small uncertainty in $pK_{i,z}$ of <0.026 at I = 100 mM (see eq(17). Therefore, in this study, we adopt constant values of 1.5 dm$^{3/2}$ mol$^{-1/2}$ for aD and 0.1 dm^3 mol^{-1} for b for all temperatures.

To evaluate degree of ionization of species i, we use the apparent equilibrium constant, $\tilde{K}_{i,z}(T)$, which accounts for both, temperature and ionic strength effects, in the electroneutrality condition:[52]

$$\sum_{i=1}^{s}c_i\sum_{z=n_i}^{p_i}zg_{i,z}(T) + c_H - \frac{\tilde{K}_W(T)}{c_H} = 0 \tag{20}$$

where $g_{i,z}(T) = L_{i,z}(T)c_H^z/\sum_{z=n_i}^{p_i}L_{i,z}(T)c_H^z$ is the dissociation level of the species i, c_i is the total concentration, and $\tilde{K}_W(T) = K_W(T)/\gamma_H(T)\gamma_{OH}(T)$ is the apparent equilibrium constant of water. Outside of the safe[50] pH range (pH of 5 to 9), one must take into account the variation in water equilibrium constant, $K_W(T)$, with temperature to accurately determine the concentration of OH$^-$ and H$^+$, and their contribution to conductivity. In the current model, we used the water properties $pK_W(\theta)$, $\Delta H^{\circ}_W(\theta)$ and $\Delta C^{\circ}_W(\theta)$ reported by Olofsson and Hepler.[58] $L_{i,z}(T)$ depends on the apparent equilibrium constants as given by Bercovici et al.[52]

$$
L_{i,z}(T) =
\begin{cases}
\displaystyle\prod_{z'=z}^{-1}\tilde{K}_{i,z'}(T) & z < 0 \\
1 & z = 0 \\
\displaystyle\prod_{z'=0}^{z-1}\tilde{K}_{i,z'}^{-1}(T) & z < 0
\end{cases}
\tag{21}
$$

Solution Method for Temperature Model. Equations 5, 16, 17, 18, 20, and 21, therefore, constitute our temperature effects model for effective mobility including the temperature effects on viscosity, ion solvation, ionic strength correction, and degree of ionization. To solve this system, we first solve for the thermodynamic equilibrium constants of each species at the operating temperature using eq 16, and then we propose an initial guess for c_H. We take as an initial guess simply the solution of the eq 20 with zero ionic strength, and use this to calculate the ionic concentrations, $c_{i,z}$ activity coefficients, $\gamma_{i,z}(T)$, and apparent equilibrium constants, $\tilde{K}_{i,z}(T)$ as per eqs

17, 18, and 21. Then, eq 20 is solved repeatedly for $c_{i,z}$ by Newton iteration, until the solution for c_H converges to a value within a predefined tolerance. Similar solution methods were adopted by Bercovici et al.[52] and Bahga et al.[42]

The ionic strength obtained through this process is then used to calculate the fully ionized actual mobility, $\mu_{i,z}(T)$, of every ionic species at the operating temperature, T, using our version of extended (and modified) Onsager–Fuoss expression, eq 5, which accounts for viscosity, ion solvation, and ionic strength effects with temperature. This actual mobility of species i is then corrected to the effective mobility, as given by

$$\mu_i(T) = \sum_{z=n_i}^{p_i} \mu_{i,z}(T) g_{i,z}(T) \tag{22}$$

using the temperature dependent dissociation factor, $g_{i,z}(T)$.[52]

Quantifying the Aggregate Effect of Temperature Dependences Unrelated to Viscosity. In this study, we address all major physical phenomena associated with the temperature dependence of electrolyte mobility in water. The easiest, most common, and often most pronounced effect to take into account is the temperature dependence of viscosity of water. We introduce factor f, which normalizes the electrolyte solution conductivity by the change associated with variations in viscosity as follows:

$$f = \frac{\sigma(\theta)\eta(\theta)}{\sigma(T)\eta(T)} \tag{23}$$

Here, conductivity, σ, is defined as

$$\sigma(T) = \sum_{i=1}^{s} c_i \sum_{z=n_i}^{p_i} Fz\mu_{i,z}(T) g_{i,z}(T) \tag{24}$$

f therefore quantifies the aggregate effect of all phenomena other than simple changes in solvent viscosity. Namely, f describes the net effect on conductivity due to temperature-dependent changes in degree of ionization, ion solvation, and ionic strength corrections. An ideal ion which follows Walden's rule exactly has an f value of unity ($\log_{10} f = 0$). The sign of $\log_{10} f$ indicates if these effects act in concert with or against the influence of viscosity on electrolyte solution conductivity (these effects oppose the influence of viscosity on buffer conductivity with positive $\log_{10} f$). This useful parameter and its application were first proposed by Ross and Locascio[15] in 2002 and is relevant for many electrophoresis effects including joule heating, dispersion, and voltage versus current requirements.

Stand-Alone Simulation Tool for Temperature-Dependent Electrolyte Properties. We developed a MATLAB (R2012b Mathworks, Natick, MA) based simulation tool for electrolyte solutions which incorporates our comprehensive temperature model. This simulation tool inputs mobilities and thermophysical data and calculates system pH, system conductivity, and effective mobilities for arbitrary mixtures of strong or weak electrolytes. The electrophoretic mobilities of all analytes presented in this study (except water ions) were obtained from Hirokawa et al.[59] The ionization dissociation constants, $pK_{i,z}(\theta)$, standard molar enthalpy change, $\Delta H_{i,z}^{\circ}(\theta)$, and standard molar heat capacity change, $\Delta C_{p,i,z}^{\circ}(\theta)$, of each species were obtained from Goldberg at al.[41] (see also Supporting Information). We also offer an extended list of analytes with their chemical properties built into a graphical user interface of the Matlab script. When available, we list all four of the chemical properties. However, for the some ionic

species, data on $\Delta C_{p,i,z}^{\circ}(\theta)$ is not available, in which case, we list only the mobility, $\mu_{i,z}(\theta)$,[59] $pK_{i,z}(\theta)$,[54] and $\Delta H_{i,z}^{\circ}(\theta)$.[54] Our code, which we named Simulation of Temperature Effects on Electrophoresis (STEEP), is available for free on our Web site at http://microfluidics.stanford.edu/download/index.html. We include source code, a database of thermophysical data, and instructions for use.

MATERIALS AND EXPERIMENTAL METHODS

To experimentally validate our model, we explored temperature effects on buffer conductivity and pH as these are the most generally applicable consequences of the model. As we shall see, these measurements can be used to illustrate each of the effects we model, including degree of ionization and ion solvation. We note that mobilities of individual analytes can be most strongly affected by temperature, but individual analyte mobilities are typically ad hoc and useful to a specific application. We further discuss examples of analyte mobility prediction in the Supporting Information. For example, in Section S-5 we discuss a case where the temperature trends of three background buffers determine whether the mobility of a single analyte increases dramatically, decreases, or stays approximately the same with increasing temperature. In Section S-6 we given an example of how three analytes can have very distinct temperature trends in a single background buffer.

We chose to summarize our experimental validation using the four two-component electrolyte solutions shown in Table 3. (In Supporting Information, we provide list of six additional solutions we analyzed experimentally in our study.) In each case, we prepared three replicates of each electrolyte solution in a 50 mL Erlenmeyer flasks. We placed each sample on a magnetic stirrer and hot plate (Fisher Scientific, Isotemp). We inserted a carbon conductivity probe (Corning Model 541P) into the flask, and sealed it with parafilm to minimize the effects of evaporation on the ion concentrations. The conductivity and temperature were measured during both heating and cooling between 25 and 70 °C in approximately 5 °C increments using a Corning Pinnacle 542 conductivity meter. We calibrated the conductivity probe prior to each measurement set using conductivity standards purchased from Ricca Chemical Company. Using the system's Pinnacle "3 in 1" Premium Gel Combo electrode, we also measured the pH of each electrolyte solution at 25 and 70 °C. Data obtained during either heating or cooling track each other closely, consistent with negligible hysteresis effects in our method.

RESULTS AND DISCUSSION

Predictions of Effective Mobility, Conductivity, and pH. To demonstrate our model, we selected three example buffers which demonstrate the phenomena discussed in Theory. Figures 1–3 show plots of the effective mobility of the titrating anion for temperatures from 20 to 80 °C, with respect to its effective mobility at the reference temperature, θ = 25 °C, as follows: $\mu_-(T)/\mu_-(\theta)$ (the subscript indicates an anion). The curves associated with our full temperature model (including all effects considered here) are labeled "current". In the upper insets of Figures 1–3, we show predictions of the full temperature model for the anion and cation pKs and electrolyte solution pH as functions of temperature. In the lower insets, we show plots of ionic strength, I, and normalized electrolyte solution conductivity, f, as functions of temperature.

5108

dx.doi.org/10.1021/ac400447k | *Anal. Chem.* 2013, 85, 5103–5113
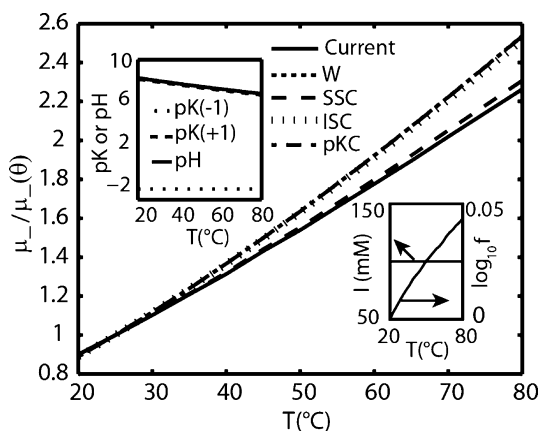
Figure 1. Predicted electrophoretic mobility of Cl⁻ in a solution containing 200 mM Tris and 100 mM HCl. The pH of this simple buffer tracks closely the temperature dependent value of pK as expected. However, the degree of Tris ionization is determined by the chloride ion whose molar density is insensitive to pH. Therefore, this electrolyte system maintains constant ionic strength with temperature. The simple SSC model is fairly accurate here which suggest that the source of the nonviscosity related temperature dependence is due to the change in the hydration shell of the chloride ion.
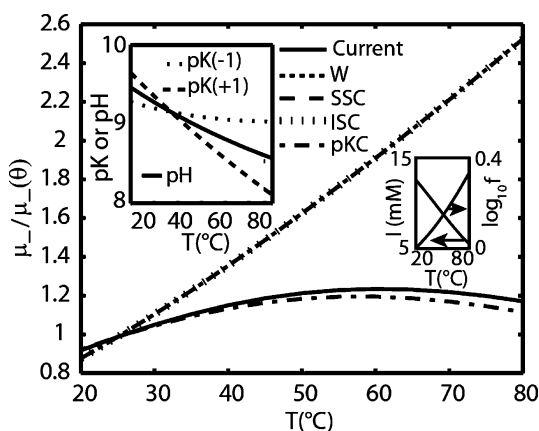
Figure 2. Predicted electrophoretic mobility versus temperature of boric acid anion (borate) in a solution containing 20 mM ethanolamine and 20 mM boric acid. Increase in temperature results in strong drop in pK of ethanolamine and a moderate drop in the pK of boric acid, resulting in an overall decrease in pH (top inset). Here, the most prominent contribution to both anion mobility and ionic strength, I (bottom inset) is due to the sharp decrease in degree of ionization of boric acid (hence the proximity of pKC model to current). The large, positive value of $\log_{10} f = 0$ (bottom inset) shows how this effect opposes contributions from the decreasing viscosity to conductivity. Ultimately, these opposing effects are also reflected by the shallow mobility curve (main plot). Predictions based on Walden's rule here overestimate the anion mobility by 116% (and buffer conductivity by 106%).

The main plots of Figures 1−3 also include four additional curves, which we use to demonstrate the effect of individual physical phenomena described in Theory. These curves represent incomplete versions of our model, and are described in Table 2. All curves correct for changes in water viscosity. The simplest model, W, uses only the Walden's viscosity correction term, α, to evaluate effective mobility at elevated temperature. Model SSC captures the temperature dependence of limiting ionic mobility due to changes in solvation, but disregards changes in degree of ionization and the temperature sensitivity
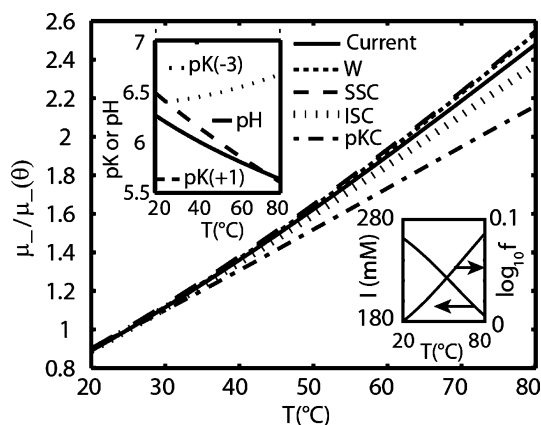
Figure 3. Predicted electrophoretic mobility of a trivalent ion, citrate, in a solution containing 200 mM Bis-tris and 50 mM citric acid. For simplicity we show only the pK of the trivalent anion of citric acid (citrate ion, $z = -3$). Increase in temperature results in a strong drop in pK of Bis-tris and a mild increase in the pK of citrate ion, resulting in an overall reduction in pH (top inset). The sharp decrease in the degree of ionization of the citrate ion contributes strongly to the decrease in ionic strength (bottom inset), which would suggest a considerable effect on its effective mobility (see limiting model pKC). However, the ion's multivalent nature makes citrate extremely sensitive to changes in the ionic strength. Therefore, the temperature-induced reduction in ionic strength is accompanied by a reduction in the magnitude of the Onsager−Fuoss correction term. These two effects largely offset each other.

of ionic strength corrections. Model ISC quantifies the temperature dependence of the extended Onsager−Fuoss and the extended Debye−Huckel theory, but the degree of ionization and the ion solvation correction terms are to always equal the value at room temperature. Model pKC, captures the temperature effects on degree of ionization, but assumes that ion solvation and ionic strength corrections are temperature insensitive.

Figure 1 shows predictions for a simple, two-component buffer consisting of a univalent weak electrolyte, 200 mM Tris, and a univalent, strong titrant anion donated by 100 mM HCl (pH = 8.18 at $\theta = 25 \,°C$). The main plot shows Cl⁻ mobility normalized by its value at the reference temperature, θ. The anion mobility increases monotonically from 20 to 80 °C. We see that the comparison curves W, ISC, and pKC each overpredict anion mobility by about the same amount, while the SSC model matches the prediction quite closely. Here, the water viscosity has the most prominent influence on the effective mobility of the chloride ion. The most dominant, nonviscous related effect is due to changes in the solvation of Cl⁻. The Stokes radius of Cl⁻ increases with temperature resulting in reduction of its absolute electrophoretic mobility. The top inset plot shows that the buffer pH tracks closely the pK of the buffering Tris, as expected, since the titrant ion Cl⁻ is donated by a strong acid so the ionization of Tris is independent of pH. For the same reason, the ionic strength of the solution (lower inset) is constant (since dissociation of Tris is determined by the concentration of the pH-insensitive Cl⁻). The slight overprediction by the SSC model is associated with a mild temperature sensitivity of the Onsager−Fuoss correction. Overall, we note that simple buffers consisting of a weak electrolyte titrated with a strongly ionized (titrant) ion typically have uniform ionic strength but have a pH change

Table 2. Summary of Full Model (Labeled Current in Figures 1−3) and Limiting Models Used for Comparing the Various Sources of Temperature Effects on Effective Ionic Mobility[a]

	effective mobility at operating temperature, T	assumptions
current	$$\mu_i(T) = \sum_{z=n_i}^{P_i} \mu_{i,z}(T) g_{i,z}(T)$$	
W	$$\mu_i(T) = \alpha \sum_{z=n_i}^{P_i} \mu_{i,z}(\theta) g_{i,z}(\theta)$$	$\beta_{i,z} = 1$, $dpK/dT = 0$, IS corr. $\neq f(T)$
SSC	$$\mu_i(T) = \alpha \sum_{z=n_i}^{P_i} \beta_{i,z}\mu_{i,z}(\theta) g_{i,z}(\theta)$$	$dpK/dT = 0$, IS corr. $\neq f(T)$
ISC	$$\mu_i(T) = \sum_{z=n_i}^{P_i} \mu_{i,z}(T) g_{i,z}(T)$$	$\beta_{i,z} = 1$, $dpK/dT = 0$
pKC	$$\mu_i(T) = \frac{\sum_{z=n_i}^{P_i} \mu_{i,z}(\theta) g_{i,z}(\theta)}{(\sum_{z=n_i}^{P_i} \mu_{i,z}(\theta) g_{i,z}(\theta))_{(I=0)}} \sum_{z=n_i}^{P_i} (\mu_{i,z}(T) g_{i,z}(T))_{(I=0)}$$	$\beta_{i,z} = 1$, IS corr. $\neq f(T)$

[a]The values $\mu_{i,z}(\theta)$ and $\mu_{i,z}(T)$ are evaluated using eq 22. $g_{i,z}(\theta)$, and $g_{i,z}(T)$ are evaluated using eq 20. The assumptions made for the limiting models include temperature insensitivity of ion solvation, ($\beta_{i,z} = 1$), temperature-independent degree of ionization ($dpK/dT = 0$), and temperature independent ionic strength corrections (IS corr. $\neq f(T)$)". T is the operating temperature and θ is the reference temperature (25°C).

with temperature dictated by the $pK(T)$ function of the weak electrolyte.

Figure 2 shows a more interesting case of a two component, weak-electrolyte buffer composed of 20 mM ethanolamine ($pK = 9.498$) and 20 mM boric acid ($pK = 9.237$). Here, the model predicts a shallow, roughly parabolic anion mobility curve with a local maximum near $T = 60$ °C. We see the comparison curves W, SSC, and ISC all track each other closely but grossly overpredict the rise in conductivity. Model pKC matches well with the comprehensive model (current), suggesting that the temperature-induced decrease in degree of ionization is primarily the source of the observed mobility behavior. This conclusion is supported by the pK and pH trends shown in the upper inset, which show that the temperature dependence of ethanolamine pK is much stronger than that of borate. As temperature is increased, the buffer pH therefore decreases faster than the pK of borate. The anion and cation pK values are each, at room temperature, close to and bound the solution pH. The dominant effect of temperature on the ethanolamine pK causes a steep drop in pH. This decreases the ionization of borate ion, thereby decreasing its effective mobility. The associated drop in the ionic strength (bottom inset), I, also influences the effective mobility by decreasing the magnitude of the Onsager−Fuoss correction (which explains the slight underprediction of pKC model from Current). Again, the large, positive value for $\log_{10} f$ (up to $\log_{10} f = 0.33$ or $f = 2.2$ at $T = 80$ °C) shows how these effects act together to strongly compensate for the decrease in water viscosity. These predictions show a discrepancy between the full model and of the Walden model by as much as 116% for the anion mobility.

Figure 3 shows an electrolyte solution composed of 200 mM Bis-tris ($pK = 6.484$) and 50 mM citric acid ($pK_{-3} = 6.396$, $pK_{-2} = 4.761$, $pK_{-1} = 3.128$). At room temperature, the pH is ~6.2, so for simplicity, we only plot the pK of its trivalent anion (citrate). Here again the model predicts that citrate mobility increases monotonically from 20 to 80 °C temperature range. The comparison curves ISC and pKC underpredict the rise in mobility, while curves W and SSC overpredict it slightly. The top inset shows that the pK of citrate increases moderately while the pK of Bis-tris drops sharply with increasing

temperature, resulting in a 0.6 pH unit drop over the temperature range. The decrease in pH results in an overall strong decrease in ionic strength by promoting reassociation of the citrate ion with hydrogen. However, the effective mobility of the trivalent citrate is only mildly reduced, because a decrease in ionic strength also strongly attenuates ionic strength effects on mobility. Interestingly, in this system including a multivalent electrolyte, the two effects ($pK(T)$ affecting dissociation and ionic strength on mobility) largely offset each other.

Temperature Model Validation. We validated our model using conductivity and pH measurements in the temperature range of 25−70 °C for the two-component electrolyte solutions listed in Table 3. For convenience of presentation, we present the data in terms of the f factor, which quantifies temperature dependence that is not attributed to variations in water viscosity (see Theory). Presentation of the experimental data in terms of f therefore also offers a direct comparison with the commonly applied Walden's rule. We also plot the conductivity for each temperature, T, with respect to conductivity evaluated at the reference temperature, θ, as follows: $\sigma(T)/\sigma(\theta)$, where $\theta = 25$°C. Similar to the discussions of Figures 1−3, the Supporting Information contains detailed discussion on the underlying physical phenomena governing the observed conductivity behavior of these solutions.

The data of Figure 4 is a compact summary of our conductivity measurements and model validation. As mentioned earlier, we prepared three replicates for each chemistry and measured electrolyte solution conductivity as a function of temperature from $T = 25$ to 70 °C. Shown in Figure 4 are the raw data for all runs. The data points cluster into groups of three since exactly revisiting each temperature value was difficult across buffer runs given our measurement method. In many cases, the three measurements overlap enough such that they are approximately indistinguishable—showing the high degree of reproducibility across replicate experiments. For all cases, we also decreased temperature from $T = 70$ °C down to $T = 25$ °C and measured conductivity at 5 °C increments (not shown here) to ensure our experiment showed no hysteresis effects (e.g., due to unwanted evaporation of water during the run). None of the data demonstrated a dependence on the sign
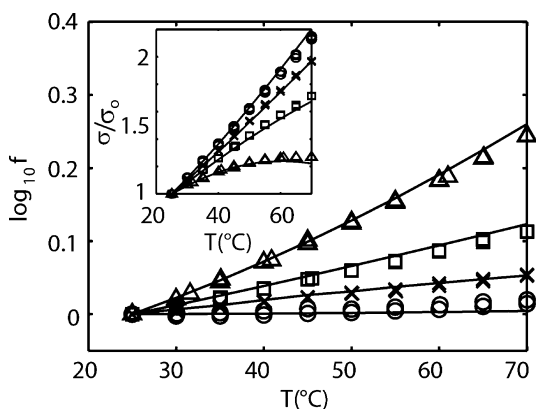
Figure 4. Experimental validation of the temperature model. Shown are theory curves along with respective conductivity (σ) measurements (raw data). The measurements are three realizations per condition (symbols clustered at each temperature) for the following electrolyte solutions: 20 mM ethanolamine and 20 mM boric acid ($\triangle$), 200 mM Bis-tris and 50 mM citric acid ($\times$). 30 mM Tris and 15 mM HEPES ($\square$), and 30 mM Tris and 15 mM acetic acid ($\bigcirc$). The factor f is defined as $\sigma(\theta)\eta(\theta)/(\sigma(T)\eta(T))$, where θ = 25 °C, and is dynamic viscosity. For the ethanolamine buffer, Walden's rule prediction for σ at 70 °C would result in 75% error.

of temperature increase. Shown together with the raw data are predictions from the current, full temperature model (solid curve).

In Figure 4, the solution of ethanolamine and boric acid (parabola) shows conductivity which is concave down and parabolic similar to the predicted anion mobility curve shown in Figure 2. The conductivity increases by a maximum of only 25%, due to the steep decline of ionization of both borate and ethanolamine ions (c.f. Figure 1 for more details). The solutions Bis-tris-potassium citrate and Tris-hepes also show increases in conductivity, but with shallower slopes, and associated higher values of $\log_{10} f$. The Bis-tris and potassium citrate conductivity changes are influenced mostly by the change in solvation of the potassium ion and by the temperature dependence of the ionic strength corrections (citrate is trivalent and therefore its mobility is very sensitive to ionic strength, see Figure S-1). The conductivity dependence of Tris-hepes is dominated by the change in degree of ionization of its constituent weak electrolyte ions (see Figure S-2 for more details). The conductivity increases by 70% for Tris-hepes and by 100% for Bis-tris and potassium citrate (from T = 25 °C to T = 70 °C). The electrolyte mixture of Tris and acetic acid has the strongest temperature dependence. We see that this buffer also shows the smallest and nearly constant values of $\log_{10} f$, suggesting that this buffer's temperature dependence is mostly due to the Walden type dependence (Figure S-3). In all four electrolyte solutions, the highlighted effects oppose the

influence of viscosity (Walden) on conductivity (positive $\log_{10} f$). At T = 70 °C, Walden's rule would yield the following errors in prediction of our measured conductivity values: 75%, 13%, 30%, and 4% for the solutions in Table 3, respectively.

For all temperatures, our electrolyte simulation tool was able to accurately predict conductivity and pH within 10% and ~0.1 pH units, respectively. We attribute a large fraction the discrepancy between data and prediction to small errors in pipetting and dilution. For example, at room temperature, the conductivity predictions for some electrolyte solutions were off by as much as 6%. If we correct our conductivity data to account for this offset at room temperature, then our conductivity prediction is within approximately 4% for all temperatures (20 °C to about 70 °C).

We measured the temperature dependence of conductivity and pH in detail for ten electrolyte solutions, and we summarize measurements associated with the additional six solutions in the Supporting Information. The latter additional solutions include sodium phosphate, Tris-HCl, Bis-tris-MOPS, sodium phosphate, histidine-acetate, and Tris-borate buffers. With the sole exception of Tris-borate buffers, the conductivity and pH predictions agreed to measured values within 4% and 0.2 pH units or better. These data suggest the model can accurately predict the temperature dependence of electrolyte solution conductivity for all the electrolyte solution explored, again with the exception of Tris-boric acid. Interestingly we are able to well predict the behavior of Tris and of boric acid when these species are paired with other ions we explored. However, the particular combination of Tris and boric acid consistently showed large discrepancies between model and measurements of conductivity and pH (respectively, 17−68% and as much as 0.32 pH units). We hypothesize that Tris and boric acid ions may undergo nonacid/base reactions with each other (see Supporting Information). This hypothesis is strongly supported by the work of Michov,[60] which showed that Tris-borate buffers contain a cyclic complex compound of betainic structure, and a buffer with both of these ions therefore does not obey the Henderson−Hasselbalch equation.

Assay Design Guidelines for Electrophoretic Separation. Joule heating is well-known to limit separation time[1] and induce significant dispersion in electrophoretic separations.[17,61] To minimize effects of Joule heating we recommend buffers that limit conductivity increase with temperature (i.e., high f factor buffers).

Temperature can also be used to improve resolution.[5−11] Separations in buffers with high magnitude dpH/dT can leverage the differences between analyte pKs (here varying temperature can increase the mobility of one analyte more than another). On the other hand, separations in buffers which maintain constant pH can leverage differences in analyte dp$K$/dT (differentially titrating one analyte versus another). See

Table 3. Experimental Validation of the Temperature Model for Electrolyte Solution pH at 25 and 70 °C[a]

		pH (T = 25 °C)		pH (T = 70 °C)	
electrolyte solution		data	theory	data	theory
20 mM boric acid	20 mM ethanolamine	9.37 ± 0.09	9.37	8.63 ± 0.09	8.68
50 mM potassium citrate	200 mM Bis-tris	9.6 ± 0.3	9.73	8.9 ± 0.1	9.01
30 mM HEPES	30 mM Tris	7.82 ± 0.02	7.82	7.0 ± 0.1	7.04
15 mM acetic acid	30 mM Tris	8.1 ± 0.1	8.12	7.04 ± 0.04	7.07

[a]Uncertainty values indicate 95% confidence on the mean.

Supporting Information for more details, particularly sections S-5 and S-6.

Prediction of EOF from first principles is still an unsolved problem in physics,[36,62] and correlations for EOF mobility tend to apply only to a particular combination of wall chemistry and electrolyte chemistry. This makes any generalized model for temperature effects on EOF, even empirical correlations, extremely difficult.[61,62] EOF suppression methods effective at elevated temperature have been presented and we cite them here for convenience.[5,24,63]

CONCLUDING REMARKS

We have developed and experimentally validated an electrolyte solution simulation tool which can be used to predict the effects of temperature on (1) viscosity, (2) ionic strength, (3) degree of ionization (pK), and (4) ion solvation effects on mobility. This fairly comprehensive temperature model is here offered as an advancement toward understanding and prediction of temperature effects on complex, multispecies electrophoresis systems. Our model leverages thermophysical data of the temperature dependence of the water viscosity; the temperature dependence of the Onsager-Fuoss model for finite ionic strength effects on mobility; the temperature dependence of the extended Debye−Huckel theory for correction of ionic activity; the Clarke-Glew generalized approach to predict the acid dissociation constant, pK, from tabulated thermodynamic properties; and species-specific, empirically evaluated correction terms for temperature-dependence of Stokes' radii of 11 common small ions. The model predictions show and experiments confirm temperature sensitivity of electrolyte solution pH, and the clear presence of nonviscosity related temperature effects on conductivity. For some electrolytes, the temperature induced reduction in degree of ionization strongly compensates for decreases in water viscosity, resulting in moderate conductivity increases (and even local maxima) with increasing temperature. For other electrolyte solutions, viscosity remains the dominant source of temperature dependence of conductivity, but pH can still vary significantly. Walden's rule alone can lead to large errors.

ASSOCIATED CONTENT

ⓈSupporting Information

Additional material as described in the text. This material is available free of charge via the Internet at http://pubs.acs.org.

AUTHOR INFORMATION

Corresponding Author

*E-mail: juan.santiago@stanford.edu. Fax: 650-723-7657

Notes

The authors declare no competing financial interest.

ACKNOWLEDGMENTS

REFERENCES

(1) Landers, J. P. *Handbook of Capillary Electrophoresis*, 2 ed.; CRC Press, Taylor and Francis Group, LLC: Boca Raton, FL, 2008.

(2) Liang, D.; Chu, B. *Electrophoresis* **1998**, *19* (14), 2447−2453.

(3) Liu, S.; Shi, Y.; Ja, W. W.; Mathies, R. A. *Anal. Chem.* **1998**, *71* (3), 566−573.

(4) Zhang, J.; Fang, Y.; Hou, J. Y.; Ren, H. J.; Jiang, R.; Roos, P.; Dovichi, N. J. *Anal. Chem.* **1995**, *67* (24), 4589−4593.

(5) Kelly, L.; Nelson, R. J. *J. Liq. Chromatogr.* **1993**, *16* (9−10), 2103−2112.

(6) Smith, S. C.; Khaledi, M. G. *Anal. Chem.* **1993**, *65* (3), 193−198.

(7) Lin, C.-E.; Chang, C.-C.; Lin, W.-C. *J. Chromatogr. A* **1997**, *768* (1), 105−112.

(8) Rasmussen, H. T.; McNair, H. M. *J. Chromatogr. A* **1990**, *516* (1), 223−231.

(9) Hoffstetter-Kuhn, S.; Paulus, A.; Gassmann, E.; Widmer, H. M. *Anal. Chem.* **1991**, *63* (15), 1541−1547.

(10) Whang, C. W.; Yeung, E. S. *Anal. Chem.* **1992**, *64* (5), 502−506.

(11) Chang, H.-T.; Yeung, E. S. *J. Chromatogr. A* **1993**, *632* (1−2), 149−155.

(12) Nübel, U.; Engelen, B.; Felske, A.; Snaidr, J.; Wieshuber, A.; Amann, R. I.; Ludwig, W.; Backhaus, H. *J. Bacteriol.* **1996**, *178* (19), 5636−43.

(13) Rush, R. S.; Cohen, A. S.; Karger, B. L. *Anal. Chem.* **1991**, *63* (14), 1346−1350.

(14) Rochu, D.; Ducret, G.; Masson, P. *J. Chromatogr. A* **1999**, *838* (1−2), 157−165.

(15) Ross, D.; Locascio, L. E. *Anal. Chem.* **2002**, *74* (11), 2556−2564.

(16) Shackman, J. G.; Munson, M. S.; Kan, C.-W.; Ross, D. *Electrophoresis.* **2006**, *27* (17), 3420−3427.

(17) Grushka, E.; McCormick, R. M.; Kirkland, J. J. *Anal. Chem.* **1989**, *61* (3), 241−246.

(18) Petersen, N. J.; Nikolajsen, R. P. H.; Mogensen, K. B.; Kutter, J. P. *Electrophoresis.* **2004**, *25* (2), 253−269.

(19) Evenhuis, C. J.; Guijt, R. M.; Macka, M.; Marriott, P. J.; Haddad, P. R. *Anal. Chem.* **2006**, *78* (8), 2684−2693.

(20) Gaš, B.; Kenndler, E. *Electrophoresis* **2000**, *21* (18), 3888−3897.

(21) Ghosal, S.; Chen, Z. *Bull. Math. Biol.* **2010**, *72* (8), 2047−2066.

(22) Kestin, J.; Sokolov, M.; Wakeham, W. A. *J. Phys. Chem. Ref. Data.* **1978**, *7* (3), 941−948, DOI: 10.1063/1.555581.

(23) Nightingale, E. R. *J. Phys. Chem.* **1959**, *63* (9), 1381−1387.

(24) Evenhuis, C. J.; Hruska, V.; Guijt, R. M.; Macka, M.; Gaš, B.; Marriott, P. J.; Haddad, P. R. *Electrophoresis* **2007**, *28* (20), 3759−3766.

(25) Okamoto, H.; Mori, K.; Ohtsuka, K.; Ohuchi, H.; Ishii, H. *Pharm. Res.* **1997**, *14* (3), 299−302.

(26) Anderko, A.; Lencka, M. M. *Ind. Eng. Chem. Res.* **1997**, *36* (5), 1932−1943.

(27) Clancy, M. J. *Histochem. J.* **1987**, *19* (1), 27−34.

(28) Beynon, R. J.; Easterby, J. S. *Buffer Solutions*; IRL Press at Oxford University Press: Oxford, U.K., 1996.

(29) Fukada, H.; Takahashi, K. *Proteins* **1998**, *33* (2), 159−166.

(30) Wang, C.-K.; Tsao, H.-K. *J. Phys. Chem. B* **2004**, *108* (45), 17685−17693.

(31) Reijenga, J. C.; Gagliardi, L. G.; Kenndler, E. *J. Chromatogr. A* **2007**, *1155* (2), 142−145.

(32) Mandaji, M.; Rübensam, G.; Hoff, R. B.; Hillebrand, S.; Carrilho, E.; Kist, T. L. *Electrophoresis.* **2009**, *30* (9), 1501−1509.

(33) Milanova, D.; Chambers, R. D.; Bahga, S. S.; Santiago, J. G. *Electrophoresis* **2011**, *32* (22), 3286−3294.

(34) Diekmann, S. *Nucleic Acids Res.* **1987**, *15* (1), 247−265.

(35) Kan, C. W.; Barron, A. E. *Electrophoresis* **2003**, *24* (1−2), 55−62.

(36) Evenhuis, C. J.; Guijt, R. M.; Macka, M.; Marriott, P. J.; Haddad, P. R. *Electrophoresis.* **2006**, *27* (3), 672−676.

(37) Onsager, L.; Fuoss, R. M. *J. Phys. Chem.* **1931**, *36* (11), 2689−2778.

(38) Grenthe, I.; Wanner, H. *TDB-2 Guidelines for the Extrapolation to Zero Ionic Strength*; Osthols, E., Ed.; Agence de l'OCDE pour L'Énergie Nucléaire, OECD Nuclear Energy Agency: France, 2000.

(39) Debye, P.; Huckel, E. *Z. Phys.* **1923**, *24*, 185.

(40) Clarke, E. C. W.; Glew, D. N. *Trans. Faraday Soc.* **1966**, *62* (0), 539−547.

(41) Goldberg, R. N.; Kishore, N.; Lennen, R. M. *J. Phys. Chem. Ref. Data.* **2002**, *31* (2), 231−370.

(42) Bahga, S. S.; Bercovici, M.; Santiago, J. G. *Electrophoresis.* **2010**, *31* (5), 910−919.

(43) Walden, P.; Ulich, H.; Busch, G. *Z. Phys. Chem.* **1926**, *123*, 429.

(44) Sadek, H. *J. Electroanal. Chem. Interfacial Elechochem.* **1983**, *144* (1−2), 11−32.

(45) Fernandez-Prini, R.; Atkinson, G. *J. Phys. Chem.* **1971**, *75* (2), 239−244.

(46) Jenkins, H. D. B.; Marcus, Y. *Chem. Rev.* **1995**, *95* (8), 2695−2724.

(47) Porras, S. P.; Riekkola, M.-L.; Kenndler, E. *Electrophoresis.* **2003**, *24* (10), 1485−1498.

(48) *CRC Handbook of Chemistry and Physics*, 91st ed.; CRC Press, Taylor & Francis Group: Boca Raton, FL, 2011−2012.

(49) Robinson, R. A.; Stokes, R. H. *Electrolyte Solutions*. 2nd revised ed.; Dover Publications: New York, 2002.

(50) Persat, A.; Suss, M. E.; Santiago, J. G. *Lab Chip* **2009**, *9* (17), 2454−2469.

(51) Štědrý, M.; Jaroš, M.; Hruška, V.; Gaš, B. *Electrophoresis* **2004**, *25* (18−19), 3071−3079.

(52) Bercovici, M.; Lele, S. K.; Santiago, J. G. *J. Chromatogr. A* **2009**, *1216* (6), 1008−1018.

(53) Persat, A.; Chambers, R. D.; Santiago, J. G. *Lab Chip* **2009**, *9* (17), 2437−2453.

(54) Christensen, J. J.; Hansen, L. D.; Izatt, R. M. *Handbook of Proton Ionization Heats and Related Thermodynamic Quantities*; Wiley New York: 1976.

(55) Wright, M. R. *An Introduction to Aqueous Electrolyte Solutions*; Wiley: Chichester, U.K., 2007; pp 230−243.

(56) Lewis, G. N., Randall, M., Pitzer, K. S., Brewer, L. *Thermodynamics*, 2 ed.; McGraw-Hill: New York, 1961; p 723.

(57) Grenthe, I.; Plyasunov, A. *Pure Appl. Chem.* **1997**, *69* (5), 951−958.

(58) Olofsson, G.; Hepler, L. *J. Solution Chem.* **1975**, *4* (2), 127−143.

(59) Hirokawa, T.; Nishino, M.; Kiso, Y. *J. Chromatogr. A.* **1982**, *252*, 49−65.

(60) Michov, B. M. *Electrophoresis* **1986**, *7* (3), 150−151.

(61) Tang, G.; Yang, C.; Chai, J.; Gong, H. *Int. J. Heat Mass Transfer* **2004**, *47* (2), 215−227.

(62) Hunter, R. J. *Zeta Potential in Colloid Science: Principles and Applications*; Academic Press: London, 1981; Vol. *125*.

(63) Chiari, M.; Cretich, M.; Damin, F.; Ceriotti, L.; Consonni, R. *Electrophoresis* **2000**, *21* (5), 909−916.